



Research Paper

Effect of Organoclay on the Performance of Reverse Osmosis Membrane

Mohamed Afzal Mohamed Amin^{1,2}, Pei Sean Goh¹, Ahmad Fauzi Ismail^{1,*}¹ Advanced Membrane Technology Research Centre (AMTEC), School of Chemical and Energy Engineering, Faculty of Engineering, Universiti Teknologi Malaysia, 81310, Johor Bahru, Johor, Malaysia² Department of Chemical Engineering and Sustainability Energy, Faculty of Engineering, Universiti Malaysia Sarawak, 94300, Kota Samarahan, Sarawak, Malaysia

Article info

Received 2019-07-04
 Revised 2019-10-01
 Accepted 2019-10-02
 Available online 2019-10-02

Keywords

Organoclay
 Substrate layer
 Thin film nanocomposite membrane
 Reverse osmosis membrane

Highlights

- TFC membrane was prepared by incorporated organoclay in the substrate layer.
- Additional of organoclay significantly enhanced the hydrophilicity of the TFC membrane.
- Modified membrane exhibited high water flux without sacrificing the salt rejection.

Abstract

This study investigated the effect of Cloisite15A (C15A) organoclay in the substrate layer on the performance of reverse osmosis (RO) membranes. The substrate of the RO membranes was modified using different loading of C15A (ranging from 0.3 - 0.7 wt%) within polysulfone (PSf) substrate and the polyamide (PA) selective layer was formed on the top. Effect of the modified substrate layer on the water flux and salt rejection of the nanocomposite membrane was investigated. The chemical property, morphology, and topography of the membrane surface were characterized by ATR-FTIR, SEM, AFM and contact angle analyzer. The modified membranes showed significantly enhanced pure water flux and salt solution permeability by 60.5 % and 44.3 %, respectively, without sacrificing the salt rejection.

© 2020 MPRL. All rights reserved.

1. Introduction

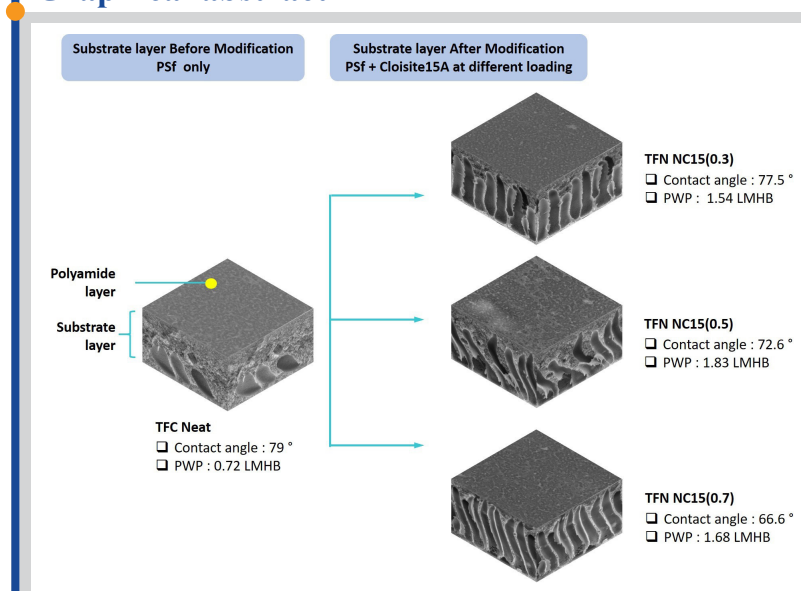
Water is the most crucial component in the life cycle of every living organism and for the development of human civilization. The accessibility of freshwater resources for human consumption is limited as most of the global water composition comes from seawater. Only 1 - 1.5% of the global water is fresh and readily accessible, whereas the rest is locked in the form of ice mostly at Arctic and Antarctica continents [1].

Desalination is an attractive alternative technology to supply clean water for domestics and industrial applications. Membrane technology has dominated the desalination market and playing an important role in clean water production. RO desalination process has developed quickly over the last three decades as the dominant membrane-based desalination technique due to

the high quality of product water. Desalination is also known as a less energy intensive technology compared to the conventionally used thermal-based desalination technology [2]. RO thin film composite (TFC) membranes composed of an outer ultra-thin PA layer and a porous support made from polymers such as polysulfone and polyethersulfone. Both layers play vital roles during the separation process where the PA layer acts a salt rejection barrier while support act as a support of the PA layer.

Many studies have proved that the performances of TFC RO membranes are mainly determined by the PA selective layer because both solute rejection and water flux performance can be tailored by solely changing the properties of this dense layer [3-5]. However, some studies have also evidenced that

Graphical abstract



* Corresponding author at: Phone: 07-5535807; fax: 07 5535625
 E-mail address: afauzi@utm.my (A.F. Ismail)

importance of substrate layer towards the overall performance of TFC RO membrane [6,7]. The physico-chemical properties of the substrate such as pore morphology and wetting property influence the formation of active layers [8,9]. Many strategies have been established to improve the intrinsic properties of the substrate. One of the most straightforward approaches is through the incorporation of nanoparticles into the polymeric substrate. The unique properties of nanomaterials can impart new functionalities to the membrane such as improving wettability of the membrane surface, suppression of macro void formation and promoting finger-like structure formation, as well as enhancing pore interconnectivity [10]. Pakizeh et al. reported that the presence of silica nanoparticles in the substrate matrix impeded the TMC diffusion during interfacial polymerization, hence a less dense PA selective layer was formed [11].

Clay-based nanomaterials have been widely studied for the preparation of nanocomposite membranes. The structural properties of clay-based materials impart significant improvement towards the performance and characteristics of the resultant nanocomposite membranes [12,13]. Abolhassan and co-workers studied the effect of different loadings of montmorillonite in the electrospun nanofibrous membranes (ENM) on the dye wastewater treatment performance in terms of mechanical strength and permeation properties [14]. Results showed that nanocomposite ENM significantly increased water flux without sacrificing the dye rejection. Lai et al. fabricated nanocomposite hollow fiber membranes by incorporating different loadings of Cloisites 30B organoclay in order to improve the membrane abrasion resistance in water treatment applications [15]. They revealed that the membrane structure as well as mechanical properties in terms of stiffness and flexibility has been improved. Palani et al. reported that the presence of montmorillonite organoclay in the polymeric structure can enhance the membrane water uptake [16]. Although this study focused on the development of fuel cell membranes, the effect of clay material on the wetting property of the membrane is interesting, especially for water treatment applications. Recently, Daraei and Ghaemi study the effect of organoclays incorporated in the polyethersulfone membrane matrix for oily water filtration [17]. In their study, it is evidenced that by introducing organoclay in the polymeric membrane, the clay nanomaterials could be well dispersed hence forming a membrane with less structural defects. The membrane also exhibited higher porosity, increased surface hydrophilicity and surface roughness as well as good mechanical strength.

Thus, in this work, predetermined amounts of C15A were incorporated into a PSf polymeric solution to fabricate the substrate layer of the PA TFN membrane. The effects of C15A on the properties of the PA selective layer as well as the RO performance are reported. This study may provide useful insights on the behaviour of water flux of the TFC RO membrane with the additional of C15A organoclay.

2. Experimental

2.1. Materials

Commercial Polysulfone (PSf, Udel P-3500, Solvay Advanced Polymers) and *N,N* dimethylformamide (DMF, AR grade, VChem) were used to fabricate the substrate layer for TFC membrane. 1,3-phenylenediamine (MPD, >99.0%, Merck) and 1,3,5-benzenetricarboxylic acid chloride (TMC, >98.0%, Acros Organic) were the monomers used for the synthesis of the polyamide (PA) membrane selective layer. The C15A (Southern Clay, USA), organically modified montmorillonite, were used as a nanofillers (Typical dry particle size: <10 μ m (d_{50}), d_{01} = 3.63nm). Sodium chloride (NaCl, crystalline, >99.0%, Merck) was used to prepare a salt solution for membrane performance. Reverse osmosis water (RO) was obtained from a Milli-Q ultrapure water purification system.

2.2. Fabrication of TFN RO membrane

2.2.1. Fabrication of the substrate layer

The PSf substrates were fabricated by using 15 wt% of PSf and different loadings of C15A organoclay (range between 0.30 - 0.70 wt.%). The process starts with the preparation of dope solution. First, C15A organoclay was mixed into the DMF solvent. Then, the solution was placed in an ultrasonic water bath for 30 minutes to fully disperse the C15A. PSf pellets were slowly added into the mixture until it was fully dissolved and homogenize. The prepared dope solution was kept at 25 °C for 24 h to remove trapped air bubbles. Next, the solution was poured on glass plates and then spread into films using a glass rod. The nascent films were immersed in a water coagulation bath in order to terminate the phase inversion process. Then, the substrate was peeled off from the glass plate and immersed to another water

bath overnight to completely remove the residual solvent before it was used for TFN FO membrane preparation.

2.2.2. Fabrication of PA selective layer

The PA layer was formed via the interfacial polymerization (IP) process between MPD and TMC on the surface of the prepared substrate membrane. At first, an appropriate volume of 2 % (w/v) MPD aqueous solution was poured on the top of substrate. Afterward, the excess MPD solution was drained off from the substrate surface and the remaining droplets were firmly removed by using rubber roller. Then, the substrate surface was filled with 0.1 % (w/v) TMC solution in n-hexane and drained off after 50 s contact time followed by drying in air at ambient condition for 1 min before proceeding to curing process at 60 °C for 5 minutes in an oven. Finally, the resultant TFC/TFN membrane was stored in RO water prior to use. These TFC/TFN membranes were coded depending on the C15A fraction in the membrane dope solution. A summary of membrane coding is shown in Table 1.

Table 1
Formulation of the TFC/TFN composite membranes

Membrane designation	Composition of membrane dope solution		
	PSf (wt%)	DMF (wt%)	C15A (wt%)
Neat	15.0	85.0	0.0
NC15(0.3)	15.0	84.7	0.3
NC15(0.5)	15.0	84.5	0.5
NC15(0.7)	15.0	84.3	0.7

2.3. Substrate and TFC/TFN characterization

The functional group of TFC/TFN membrane was identified by employing the attenuated total reflectance Fourier transmission infrared spectroscopy characterization (ATR-FTIR, Thermo Nicolet Avatar 360). The area 1 cm² of each TFC/TFN membrane was selected. Prior to analysis, the membranes were dried in a vacuum at 40 °C for 24 h. The spectra were investigated in the range of wavelengths 1800 to 800 cm⁻¹. The surface and cross-sectional structures morphology of prepared membranes were examined using scanning electron microscopy (SEM, TM3000 Hitachi Japan). The cross-section of the membrane was prepared by immersed and subsequently fracturing the membranes in liquid nitrogen. All the specimens were coated with a thin layer of platinum using a sputtering coater machine before scanned with SEM. The surface roughness of the thin film membranes was measured by atomic force microscopy (AFM) (AFM5000II Hitachi, Japan). The wetting property measurement for the dried substrate and TFC/TFN membrane were conducted using a water contact angle goniometer (OCA 15Pro, Dataphysics). An average of collected 5 readings value was reported.

2.4. Substrate and TFC/TFN membrane performance evaluation

The performance of both substrate and TFC/TFN membranes were conducted in term of permeability and selectivity using a dead-end filtration cell (Sterlitech™ HP4750) with transmembrane pressure applied at 15 bar. The permeation cell have an effective membrane area of 14.6 cm². To ensure that flux was at a steady-state condition, before the membrane undergoes performance evaluation, it was compacted at a pressure of 16.0 bar for 30 min. The substrate and TFC/TFN membranes water flux rate, J (L/m².h) will be determined using Eq. (1) as below:

$$J = \frac{\Delta V}{A_m \cdot \Delta t} \quad (1)$$

where A_m is the effective membrane area, ΔV is the permeate volume and Δt is the experimental time to collect permeate.

Salt rejection, R (%) property of the TFC/TFN membranes were determined by measuring the electrical conductivity of the permeate and the feed using 2000 ppm NaCl solution at 15 bar applied pressure. Salt solution conductivity was measured using bench top conductivity meter (Model Jenway 4520). The membrane salt rejection can be calculated using Eq. (2) as below:

$$R = \left(1 - \frac{C_p}{C_f}\right) \times 100 \quad (2)$$

where C_p and C_f are the NaCl concentration in the permeate and feed solution, respectively.

3. Results and discussion

3.1. FTIR spectra of organoclay and TFN membrane

The ATR-FTIR spectra of organoclay NC15 and TFC/TFN membranes are shown in Figure 1. The assignments of various IR absorption bands for PA, PSf and C15A were made based on literature. The FTIR spectrum of the TFC membrane shows distinct peaks of both aromatic polyamide barrier layer and PSf support layer. The peaks at 1660, 1610 and 1540 cm^{-1} attributed to C=O (amide I) stretching, hydrogen-bonded C=O (amide I) stretching, and N-H (amide II) in-plane bending, respectively, are the prominent feature for the aromatic polyamide spectrum. The characteristic PSf FTIR bands at 1585, 1245 and 1490 cm^{-1} were also present [18]. For the C15A powder, the band at 1640 cm^{-1} was related to the stretching vibrations of the quaternary ammonium salts. Whereas, the band at 1116 and 1040 cm^{-1} , can be assigned to the vibration of Si-O and Si-O-Si bonds [19]. However, the distinct peaks of the C15A do not appear in the TFN spectra at all loading. It might be due to the small fraction of C15A in the support layer that was not detected. The relative intensities of PSf and PA bands decreased with the increasing of C15A loading. The same trend has been reported by Li et al. who studied the effect of different loadings of aluminum oxide (Al_2O_3) fillers in the preparation of porous polymer membrane. They found that, when the loading of Al_2O_3 increase in polymer matrix, the intensity of two distinct spectra in the membrane decreased with the increasing amounts of Al_2O_3 nanoparticles [20].

3.2. Effect of organoclay on the membrane structure

Figure 2 illustrates SEM images of the surfaces and the cross-sections of the prepared membranes with different organoclay concentrations. The TFN exhibited greater number of pores when the C15A was introduced in the substrate layer as compared with the unmodified membrane. Similar observations has also been made for TFC membranes containing graphene oxide nanofillers [21]. The sublayer has finger-like cavities as well as a small volume of macro void structure. From the images, as the fraction of C15A in the PSf increased, the length of the membrane finger-like structure pore increased where some of them were extended to near the top of the substrate surface. Different morphology was observed for the neat membrane where it formed more spongy structure with small volume and number of microvoids as compared with the C15A loaded membrane. At 15k magnification, the spongy structure at the top of the substrate layer was looser for modified substrate as compared with the neat membrane. As for the membrane surface, the image showed a peak-and-valley and nodule-like structure. This structure is a general feature of PA TFC membranes.

Figure 3 shows the AFM topological images of neat and three different C15A incorporated substrates. As expected, the modified substrate exhibited smoother surface morphology as compared with the neat substrate. The roughness of modified substrate reduced when 0.3 wt.% of the C15A was introduced in the polymer matrix. The decrement in substrate surface roughness upon the addition of C15A organoclay most probably due to well-dispersed C15A within substrate [22,23].

Nevertheless, when the loading of C15A was further increased to 0.5 and 0.7 wt.%, the surface become rougher (9.5 and 8.3 nm respectively). Similar behavior has been reported by Hegab et al. They reported that with high concentration of graphene oxide in the TFN membrane, the roughness of the membranes increased compared to pristine membrane [24].

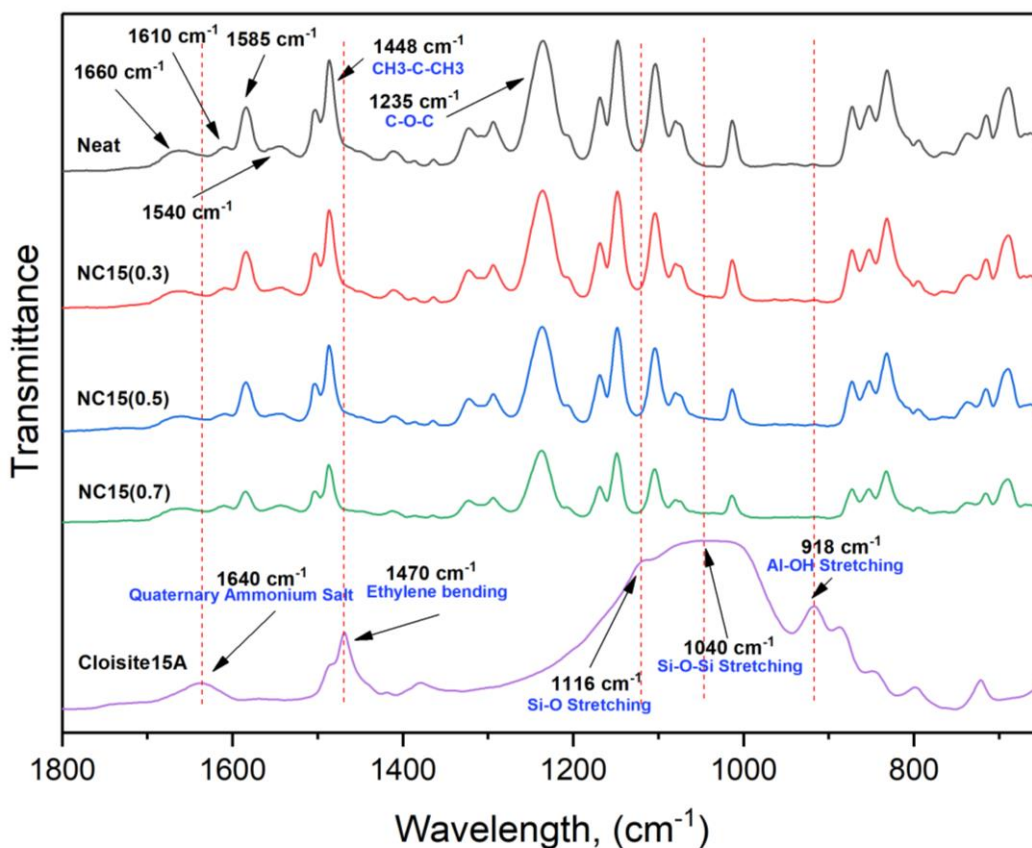


Fig. 1. FTIR profile of a Neat and NC15 (0.3 - 0.7) membranes and C15A powder, respectively.

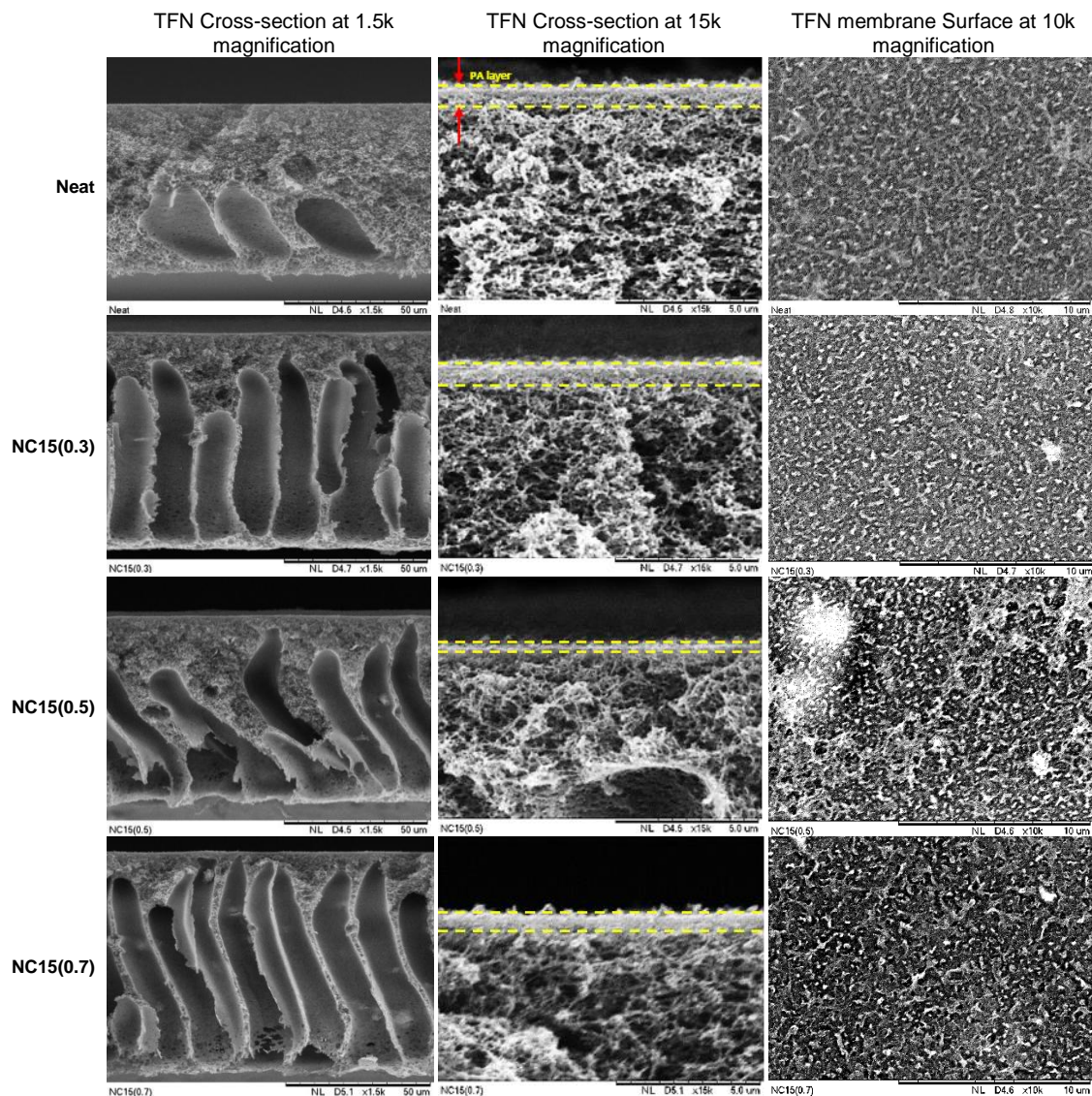


Fig. 2. Membrane cross-section at 1.5 k and 15 k magnifications and surface morphology at 10 k magnification under SEM.

3.3. Effect of organoclay on the substrate performance

The water contact angle was used to indicate the hydrophilicity and wetting characteristics of the membrane. In this study, the dynamic contact angle was executed instead of the static contact angle in which the behavior of water drop on top of the membrane surface is observed for every 50 seconds up to 700 seconds. Figure 4A shows the water contact angle of neat and modified substrates as a function of time. As can be seen, the modified substrate shows lower contact angle as compared to neat substrate. The wetting property of neat substrate reduced from 100° to 79° within 700 seconds. When C15A loading was increased from 0.3 to 0.5 wt.%, the water contact angle further decreased from 104° to 74° for substrate NC15(0.3) and from 78° to 35° for substrate NC15(0.5). The significant change in the water angle membrane indicated the improved membrane surface hydrophilicity owing to the incorporation of C15A that draws water molecules at very fast rate. Similar result has been reported by Darei and Ghanemi who also employed C15A as nanofiller [17]. As the fraction of C15A increased, the water contact angle decreased. This indicates that the addition of organoclay could enhance the hydrophilic property of the substrate because organoclay contains a large amount of hydrophilic silanol group and associated hydroxyl groups [25]. Kochkodan and Hilal also reported that, an increase in the density of surface hydrophilic-group, such as hydroxyl groups, is favorable for improving the membrane hydrophilicity [26]. However, when C15A was further increased to 0.7 wt.%, the water contact angle decreased as compared with the substrate at loading 0.5 wt.%.

Figure 4B shows pure water permeability (PWP) for all prepared

substrates. From this figure, the PWP was increased when the C15A is introduced in a PSf matrix as compared with the neat substrate. The increase in water transfer at low C15A loading can be explained by the enhancement of the substrate hydrophilicity along with the increased porous structure as compared with the neat substrate. When the C15A loading increased from 0.3 to 0.5 wt.%, the PWP showed an increment from 364.3 to 1100.7 $\text{L/m}^2\cdot\text{h}\cdot\text{bar}$. After reaching a maximum value at loading 0.5 wt.%, the PWP declined to 26% for substrate NC15(0.7). A slight lower of PWP for NC15(0.7) as compared with NC15(0.5) was due to lower chain intrusion of polymer into the clay interlayers at high clay concentration as result of high spatial limitation for clay layer expansion. In addition, the molecular diffusion into the clay gallery is generally driven by the entropy between clay particle and polymer chain confinement [12]. From Figure 4, water contact angle and PWP results showed similar trends in terms of the behavior of water transport within the substrate.

3.4. Effect of organoclay on TFC/TFN membrane

Figure 5 shows the effect of C15A on the water contact angle and PWP of the TFC/TFN membrane. Compared with the TFC membrane, TFN membranes showed improved hydrophilicity upon the incorporation of C15A. For the TFC/TFN membrane, a similar trend of PWP is evidence in Figure 5(A) and (B) as compared with the PWP for substrate whereby at 0.5 wt.% and 0.7 wt.% the PWP was increased to 60.5% and 56.8% as compared to 0.3 wt.% loading, respectively. However, at 0.7 wt.%, the PWP started to decrease due to the same reason as explained in section 3.3.

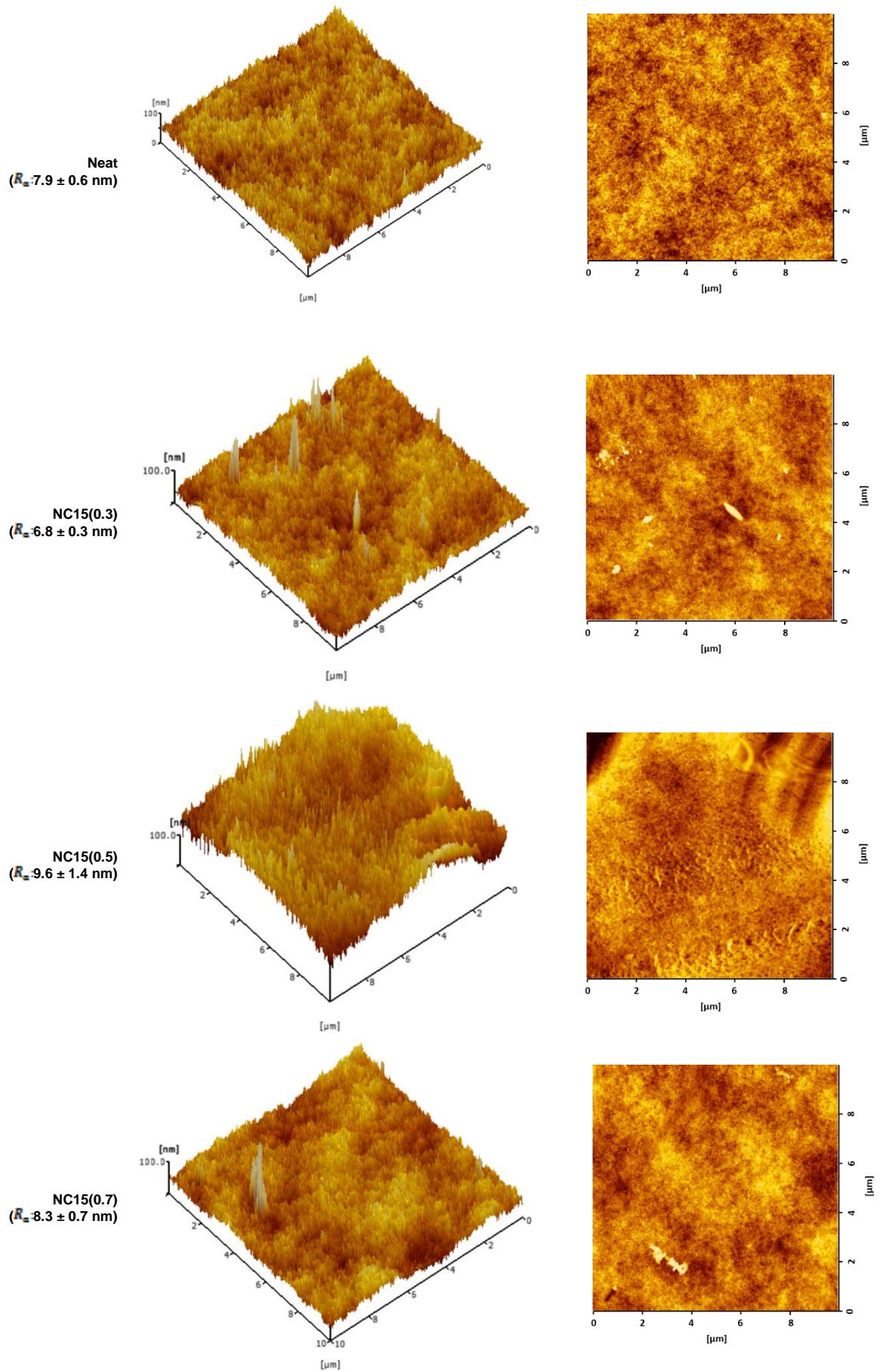


Fig. 3. 3D topographic image and 2D surface structure of Neat and NC15 (0.3-0.7) membranes.

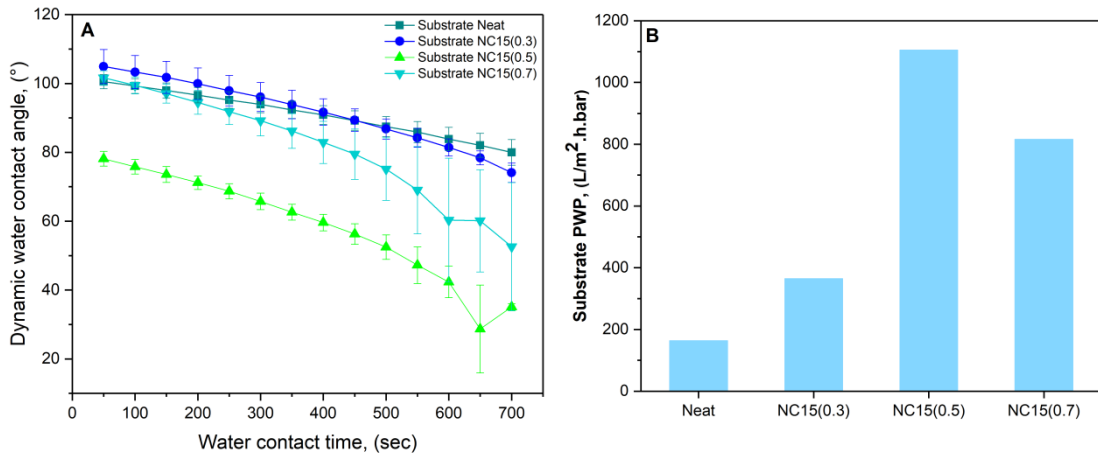


Fig. 4. (A) Dynamic contact angle trend and (B) pure water permeability for neat and modified substrates.

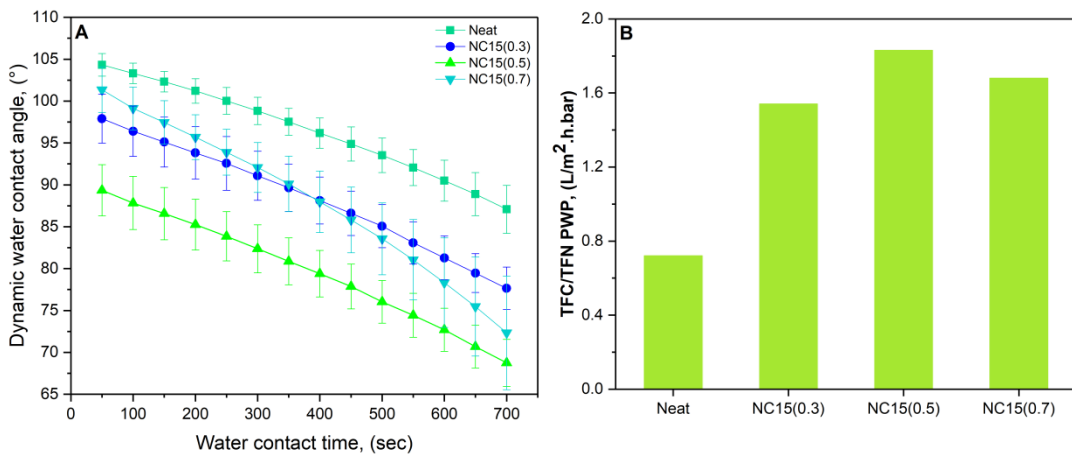


Fig. 5. A) Dynamic contact angle trend and B) pure water permeability for TFC and TFN membrane.

3.5. RO performance of TFC/TFN membrane

Figure 6 displays the RO performance test of TFC/TFN membranes with respect to solute permeability (Figure 6A) and salt rejection (Figure 6B). As can be seen from Figure 6A, the solute permeability graph showed almost similar trends with the PWP illustrated in Figure 5B. As the fraction of C15A increased from 0 to 0.5 wt %, the salt permeability shown an increment. However, when the C15A fraction was further increased to 0.7 wt %, the trends start to decrease. The TFN NC15(0.5) shows 45 % higher solute

permeability than that of TFC and other TFN membranes. Previous study reported that reduced PA layer thickness would lead to lower water transport resistance and enhanced water permeability [27]. From Figure 2, the formation of PA selective layer for NC15(0.5) was thinner as compared with other prepared membranes. With respect to rejection capability, it is found that all membranes can reject high NaCl salt by more than 95 % (refer Figure 6B). This finding indicated that the incorporation of clay has favorably increased the permeability of membrane, without affecting the salt rejection.

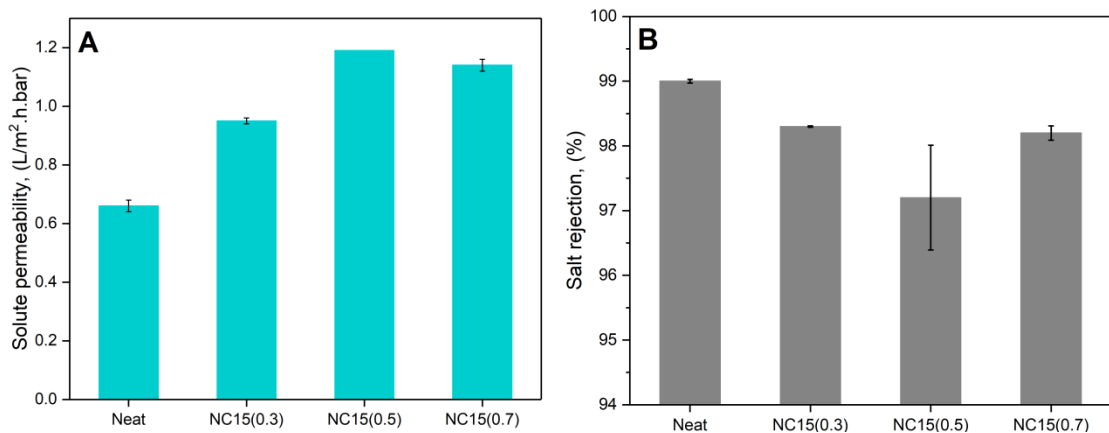


Fig. 6. Filtration behavior of the TFC/TFN membranes using the RO dead-end filtration module in term of A) Solute permeability and B) Salt rejection.

6. Conclusions

The performance of TFC RO membrane incorporated with C15A organoclay in term of water permeability and solute rejection have been studied in this research. Based on the results, it showed that, by adding the C15A in the PSf substrates matrix, the hydrophilicity of the TFC membrane improved by 20% due to the surface hydrophilic-groups. The resultant membrane exhibited higher water permeability without compromising salt rejection. The additional of organoclay in the membrane matrix has improved the water transport as it can promote more water pathway by creating extra void space for water transport. Membrane SEM morphology revealed that more finger-like structure pores were formed when C15A was added in the substrate. The porous nature of the substrates had played an important role in influencing the water transport behavior of the TFC membranes. Overall, additional C15A organoclay can enhance the physicochemical properties of the PSf substrate as well as PA selective layer with respect to surface hydrophilicity, roughness, and morphology. As a conclusion, the additional of C15A organoclay has a potential to enhance both membrane water permeability and salt rejection.

Acknowledgment

The authors would like to acknowledge the Ministry of Education (MRUN Grant: 4L873) and Universiti Malaysia Sarawak for the financial support of the study.

References

- [1] A. Pandey, Freshwater Management: An Approach to Address the 21st Century Water Crisis Abstract, *Int. J. Innov. Res. Dev.* 4 (2015) 109–118.
- [2] M. Safarpour, A. Khataee, V. Vatanpour, Thin film nanocomposite reverse osmosis membrane modified by reduced graphene oxide/TiO₂ with improved desalination performance, *J. Membr. Sci.* 489 (2015) 43–54. doi:10.1016/j.memsci.2015.04.010.
- [3] S. Shultz, V. Freger, In situ modification of membrane elements for improved boron rejection in RO desalination, *Desalination*. 431 (2018) 66–72. doi:10.1016/j.desal.2017.08.021.
- [4] P. Wen, Y. Chen, X. Hu, B. Cheng, D. Liu, Y. Zhang, S. Nair, Polyamide thin film composite nanofiltration membrane modified with acyl chlorided graphene oxide, *J. Membr. Sci.* 535 (2017) 208–220. doi:10.1016/j.memsci.2017.04.043.
- [5] R. Bi, Q. Zhang, R. Zhang, Y. Su, Z. Jiang, Thin film nanocomposite membranes incorporated with graphene quantum dots for high flux and antifouling property, *J. Membr. Sci.* 553 (2018) 17–24. doi:10.1016/j.memsci.2018.02.010.
- [6] C. Ba, J. Economy, Preparation of PMDA/ODA polyimide membrane for use as substrate in a thermally stable composite reverse osmosis membrane, *J. Membr. Sci.* 363 (2010) 140–148. doi:10.1016/j.memsci.2010.07.019.
- [7] B.D. Chuan Ding, Jun Yin, Effects of Polysulfone (PSf) support layer on the performance of thin-film composite (TFC) membranes, *J. Chem. Process Eng.* 1 (2014) 1–8.
- [8] D.A. Links, Effect of the surface property of poly (tetrafluoroethylene) support on the mechanism of polyamide active layer formation by interfacial polymerization, (2012) 8998–9004. doi:10.1039/c2sm25769f.
- [9] P.S. Singh, S. V. Joshi, J.J. Trivedi, C. V. Devmurari, A.P. Rao, P.K. Ghosh, Probing the structural variations of thin film composite RO membranes obtained by coating polyamide over polysulfone membranes of different pore dimensions, *J. Membr. Sci.* 278 (2006) 19–25. doi:10.1016/j.memsci.2005.10.039.
- [10] S. Lim, M.J. Park, S. Phuntsho, L.D. Tijing, G.M. Nisola, W.G. Shim, W.J. Chung, H.K. Shon, Dual-layered nanocomposite substrate membrane based on polysulfone/graphene oxide for mitigating internal concentration polarization in forward osmosis, *Polymer*. 110 (2017) 36–48. doi:10.1016/j.polymer.2016.12.066.
- [11] M. Pakizeh, Development of a novel thin film composite membrane by interfacial polymerization on polyetherimide/modified SiO₂ support for organic solvent nanofiltration, *Sep. Purif. Technol.* 119 (2013) 35–45. doi:10.1016/j.seppur.2013.09.003.
- [12] A.K. Zuhairun, A.F. Ismail, The role of layered silicate loadings and their dispersion states on the gas separation performance of mixed matrix membrane, *J. Membr. Sci.* 468 (2014) 20–30. doi:10.1016/j.memsci.2014.05.038.
- [13] C.Y. Lai, A. Groth, S. Gray, M. Duke, Investigation of the dispersion of nanoclays into PVDF for enhancement of physical membrane properties, *Desalin. Water Treat.* 34 (2011) 251–256. doi:10.5004/dwt.2011.2888.
- [14] S. Abolhassan, M. Vossoughi, N. Mohammad, Clay-based electrospun nano fibrous membranes for colored wastewater treatment, *Appl. Clay Sci.* 168 (2019) 77–86. doi:10.1016/j.clay.2018.11.003.
- [15] C.Y. Lai, A. Groth, S. Gray, M. Duke, Enhanced abrasion resistant PVDF/nanoclay hollow fibre composite membranes for water treatment, *J. Membr. Sci.* 449 (2014) 146–157. doi:10.1016/j.memsci.2013.07.062.
- [16] P.B. Palani, Effect of modified nanoclay composite on blended PVDF/PEG electrolyte membranes for fuel cell applications, 16 (2017) 1–6. doi:10.1142/S0219581X17600420.
- [17] P. Daraei, N. Ghaemi, Synergistic effect of cloisite 15A and 30B nanofillers on the characteristics of nanocomposite polyethersulfone membrane, *Appl. Clay Sci.* 172 (2019) 96–105. doi:10.1016/j.clay.2019.03.002.
- [18] Q. Cheng, Y. Zheng, S. Yu, H. Zhu, X. Peng, J. Liu, J. Liu, M. Liu, C. Gao, Surface modification of a commercial thin-film composite polyamide reverse osmosis membrane through graft polymerization of N-isopropylacrylamide followed by acrylic acid, *J. Membr. Sci.* 447 (2013) 236–245. doi:10.1016/j.memsci.2013.07.025.
- [19] R. Scaffaro, A. Maio, Enhancing the mechanical performance of polymer based nanocomposites by plasma-modification of nanoparticles, *Polym. Test.* 31 (2012) 889–894. doi:10.1016/j.polymertesting.2012.06.006.
- [20] Z. Li, G. Su, X. Wang, D. Gao, Micro-porous P(VDF-HFP)-based polymer electrolyte filled with Al₂O₃ nanoparticles, *Solid State Ionics.* 176 (2005) 1903–1908. doi:10.1016/j.ssi.2005.05.006.
- [21] M.E.A. Ali, L. Wang, X. Wang, X. Feng, Thin film composite membranes embedded with graphene oxide for water desalination, *Desalination*. 386 (2016) 67–76. doi:10.1016/j.desal.2016.02.034.
- [22] M. Jun, S. Phuntsho, T. He, G.M. Nisola, L.D. Tijing, X. Li, G. Chen, W. Chung, H. Kyong, Graphene oxide incorporated polysulfone substrate for the fabrication of flat-sheet thin-film composite forward osmosis membranes, *J. Membr. Sci.* 493 (2015) 496–507. doi:10.1016/j.memsci.2015.06.053.
- [23] S. Qiu, L. Wu, X. Pan, L. Zhang, H. Chen, C. Gao, Preparation and properties of functionalized carbon nanotube/PSF blend ultrafiltration membranes, 342 (2009) 165–172. doi:10.1016/j.memsci.2009.06.041.
- [24] H.M. Hegab, A. Elmekawy, T.G. Barclay, A. Michelmores, L. Zou, D. Losic, C.P. Saint, M. Ginic-Markovic, A novel fabrication approach for multifunctional graphene-based thin film nano-composite membranes with enhanced desalination and antibacterial characteristics, *Sci. Rep.* 7 (2017) 1–10. doi:10.1038/s41598-017-07531-y.
- [25] X. Liu, H.Y. Ng, Fabrication of layered silica-polysulfone mixed matrix substrate membrane for enhancing performance of thin-film composite forward osmosis membrane, *J. Membr. Sci.* 481 (2015) 148–163. doi:10.1016/j.memsci.2015.02.012.
- [26] V. Kochkodan, N. Hilal, A comprehensive review on surface modified polymer membranes for biofouling mitigation, *Desalination*. 356 (2015) 187–207. doi:10.1016/j.desal.2014.09.015.
- [27] G.S. Lai, W.J. Lau, P.S. Goh, Y.H. Tan, B.C. Ng, A.F. Ismail, A novel interfacial polymerization approach towards synthesis of graphene oxide-incorporated thin film nanocomposite membrane with improved surface properties, *Arab. J. Chem.* 12 (2019) 75–87. doi:10.1016/j.arabjc.2017.12.009.